Rudziński, Ł., Cesca, S., Lizurek, G. (2016): Complex Rupture Process of the 19 March 2013, Rudna Mine (Poland) Induced Seismic Event and Collapse in the Light of Local and Regional Moment Tensor Inversion. - *Seismological Research Letters*, *87*, 2, pp. 274—284.

DOI: http://doi.org/10.1785/0220150150

THE SEISMOLOGICAL SOCIETY OF AMERICA
400 Evelyn Ave., Suite 201
Albany, CA 94706-1375
(510) 525-5474; FAX (510) 525-7204
www.seismosoc.org

Complex Rupture Process of the 19 March 2013, Rudna Mine (Poland) Induced Seismic Event and Collapse in the Light of Local and Regional Moment Tensor Inversion

by Łukasz Rudziński, Simone Cesca, and Grzegorz Lizurek

ABSTRACT

On 19 March 2013, a strong, shallow, induced seismic event struck a mining panel in the room-and-pillar Rudna copper mine in southeastern Poland. The event caused important damage at the mining tunnel and trapped 19 miners, who were safely rescued a few hours later. Although mining-induced seismicity is frequent at this mine, the 19 March event was unusual because of its larger magnitude, its occurrence far from the mining stopes, and because it was accompanied by a strong hazardous rockburst. The mining inspections following the event verified the occurrence of a rockfall with tunnel floor uplift but also recognized the presence of a faulting structure at the hypocentral location. The availability of three monitoring networks (including local and regional data, short-period and broadband seismometers, and surface and in-mine installation) presented an optimal setup to determine rupture parameters and to compare the performance and results from different installations.

We performed waveform and spectral-based analysis to infer source properties, with a particular interest to the determination of the rupture processes, using different moment tensor (MT) inversion techniques. Our results are surprisingly different, ranging from a dominant thrust mechanism, resolved at closest distances, to a collapse-type rupture, resolved at regional distances. We demonstrate that a complex rupture model is needed to explain all observations and to justify these discrepancies. The final scenario indicates that the rupture nucleated as a weaker thrust mechanism along a pre-existing weakened surface and then continued in a more energetic collapse event. The local LUMINEOS surface network has the potential to resolve both subevents but not using a standard MT decomposition. Here, we propose a new MT decomposition and an alternative MT fitting procedure that can be used to analyze the MT of collapse sources.

Online Material: Tables of regional stations and source parameters, and figure of displacement seismograms.

INTRODUCTION

The tectonic seismicity of Poland is weak and characterized by the rare occurrence of small-to-moderate natural earthquakes (e.g., Dębski *et al.*, 1997; Domański, 2007; Wiejacz and Dębski, 2009; Lizurek *et al.*, 2013). However, Poland is faced with a relevant human-induced seismicity, especially linked to hard coal (e.g., Stec, 2007), brown coal (Wiejacz and Rudziński, 2010), and copper mining (Lizurek *et al.*, 2014). Copper-mining-induced seismicity is commonly observed in southwestern Poland, at the Lubin–Głogów Copper District (LGCD). According to the local mining monitoring system and the national seismological survey by the Institute of Geophysics Polish Academy of Sciences (IGF PAS), more than 2000 events with magnitudes between 0.9 and 3.5 are recorded yearly in this district.

On 19 March 2013, an unusually strong induced seismic event struck one of the mining panels in the room-and-pillar Rudna copper mine (Fig. 1), LGCD, Poland. The seismic event was reported as possibly triggered on an inactive fault, which was well recognized by a mining geological survey (Whidden *et al.*, 2013; Lizurek *et al.*, 2014). The Rudna mining geophysical survey located the event within the Rudna mine complex, with epicentral coordinates 51.49° N, 16.08° E, depth 1.0 km, and origin time 21:09:51.9 UTC (E. Koziarz, personal comm., 2013). The event magnitude reported by the European-Mediterranean Seismological Centre was m_b 4.6. The IGF PAS estimated a local magnitude M_L 4.2 and moment magnitude M_w 3.7 (seismic moment of 3.6×10^{14} N·m). The event was widely felt in the surrounding area (Lizurek *et al.*, 2014) and was responsible for a rockburst. In consequence of this rockburst, 19 miners were trapped in the mine, all of them being successfully rescued some hours later.

Despite of frequent mining-induced seismicity affecting the area, the 19 March 2013 event was exceptional in its magnitude and consequences. The seismic event was strong enough to be recorded at different permanent regional seismological

 doi: 10.1785/0220150150

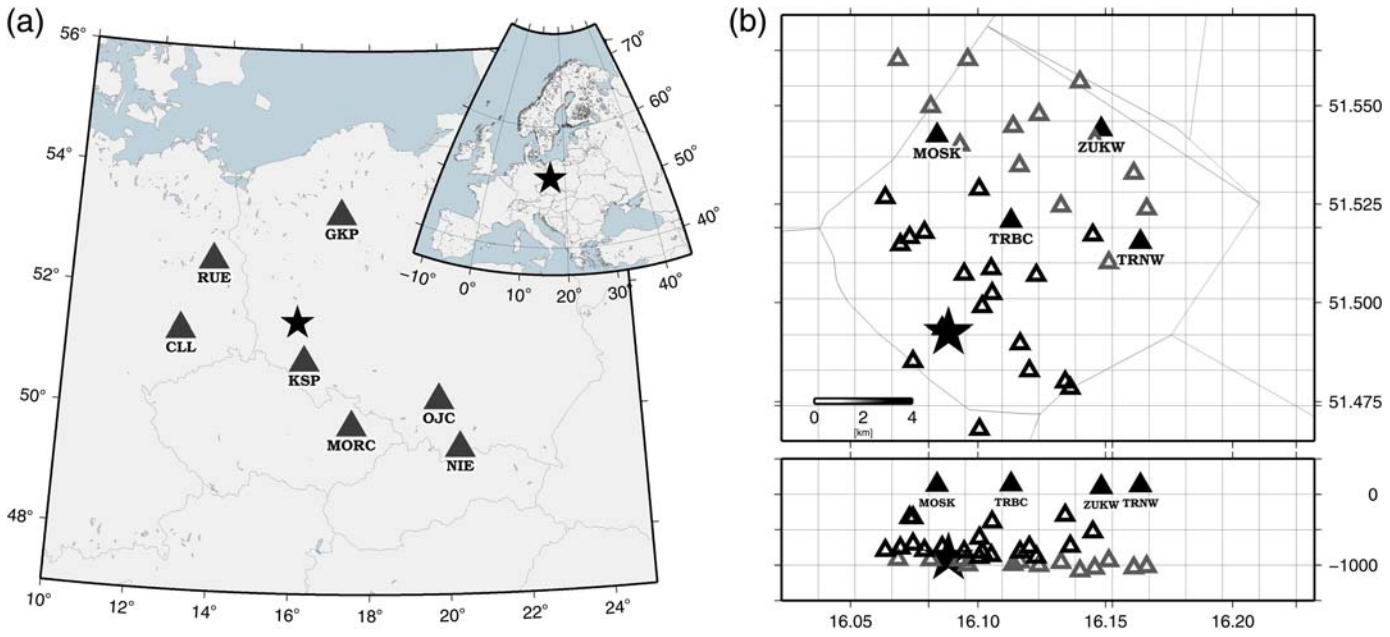

▲ **Figure 1.** Event location (star) and seismic networks: (a) regional broadband stations (inset shows broader geographic perspective), (b) surface short-period three-component stations belong to the LUMINEOS network (solid black triangles with stations codes) and short-period vertical subsurface in-mine seismic observing system (open triangles). The open black triangles denote in-mine stations located above the source, and open gray triangles show stations below the hypocenter.

stations (Figs. 1a, 2c) equipped with broadband sensors. At local distances, seismic signals were recorded by two different seismological networks devoted to the monitoring of the mines and surrounding infrastructures (Fig. 1b): the LUMINEOS and Rudna in-mine networks. The LUMINEOS surface network has an aperture of about 9 km. It is equipped with three-component short-period Lennartz LE-3D-1 s sensors with 1–100 Hz frequency range and sampling rate of 100 samples/s. On 19 March 2013, the network was still under construction, and only four seismometers were operational. The underground Rudna network has been run by the mining company since the early 1990s. The network is composed of one-component short-period Willmore MkII and MkIII seismometers with 1–100 Hz frequency band (500 samples/s), installed inside the mining tunnels at depths between 300 and 1080 m. The dynamic range is less than 70 dB, and sensors typically saturate for events with $\mathbf{M} > 3$, at which most seismograms are clipped (Fig. 2a). In these conditions, moment tensor (MT) inversion can only be performed using modeling amplitude and polarities of first arrivals. Surface installation at local and regional distances can be used instead to perform a more reliable full waveform MT inversion. The combined analysis of seismic data (see Data and Resources) of the three networks (Fig. 2 and Ⓔ Fig. S1, available in the electronic supplement to this article) provides a unique opportunity to investigate the rupture process.

The analysis of mining-induced seismic sources is of particular interest for seismologists because the underground mining environment can provide valuable information on earthquake physics in a small scale. Over the last decades, several studies focused on source mechanisms of mining events, using different inversion approaches (e.g., Gibowicz, 1990; McGarr, 1992a,b; Fletcher and McGarr, 2005; Dreger *et al.*, 2008; Lizurek and Wiejacz, 2011; Vavryčuk and Kühn, 2012; Sen *et al.*, 2013). As for tectonic events, some mining-induced earthquake sources can be well modeled by a double-couple (DC) source model (e.g., Dahm *et al.*, 1999; Richardson *et al.*, 2005). Nevertheless, most of them exhibit significant non-DC components (e.g., Dreger *et al.*, 2008; Ford *et al.*, 2009). Among the physical processes that can be described by non-DC sources, we have tensional cracks, rockfalls, collapses, and pillar bursts (Hasegawa *et al.*, 1989; Cesca *et al.*, 2013). A full MT (Jost and Hermann, 1989), able to reproduce both the effect of DC and non-DC source models, is a more general and proper representation for seismic sources in mines.

Another interesting observation of mining seismicity is that seismic recording of mining tremors are often the result of two or more subevents (e.g., Baker and Young, 1997; Cichowicz, 2000; Sprenke *et al.*, 2002; Teyssoneyre *et al.*, 2002; Malovichko, 2005; Riemer, 2005; Gibowicz, 2009). Some of these subevents are directly induced by different mining activities and induced stress perturbations, while others may be triggered along pre-existing faults or fractured regions. The correct interpretation of a full MT may still be challenging, particularly when the resolved MT is the result of the superposition of different rupture processes with different focal mechanisms.

In the present study, we investigate the complexity of the rupture process of the 19 March 2013 mining-induced seismic event by comparing MT inversion setups at local and regional distances and improving upon previous results obtained only upon the analysis of local data (Lizurek *et al.*, 2014). The com-

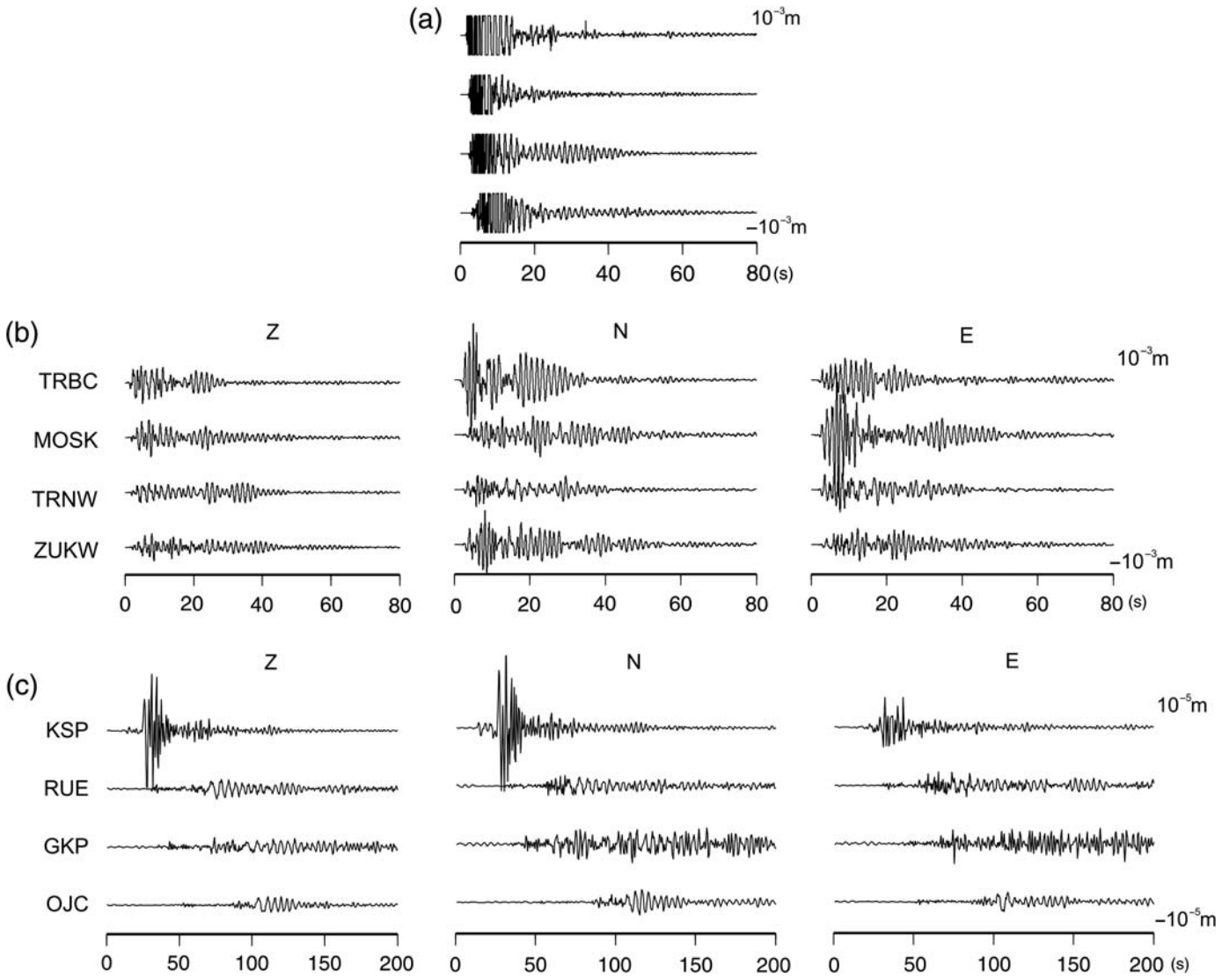

▲ **Figure 2.** Examples of displacement traces recorded on different networks: (a) four in-mine vertical seismograms with different azimuths, (b) LUMINEOS three-component recordings, and (c) regional signals recorded on different azimuths. All signals are shown in Ⓔ Figure S1.

bined interpretation of MT results leads us to infer the complex rupture history of the 19 March 2013 event.

THE 19 MARCH 2013 EVENT IN A LOCAL VIEW

Lizurek *et al.* (2014) first hypothesized that the Rudna event in March 2013 is characterized by a complex rupture. The location of the hypocenter, at some distance from the excavation room, ruled out that it was directly induced by the ongoing mining processes. On the contrary, the presence of a well-known fault zone in the vicinity of the source region suggests a case of triggered seismicity. The fault zone (Rudna Główna) was reported by miners as tectonically inactive, and the main discontinuity was mapped as a normal fault with northwest–southeast strike and slip direction to the northeast. The maximum throw observed within the mining panel was 4.5 m. The whole mining panel is located on the hanging wall of the Rudna Główna fault zone. Moreover, inside the mining panels, a few smaller normal faults of northwest–southeast and northeast–southwest strikes and throws from 0.2 to 1.6 m were mapped. Within the excavations of the panel, minor, mainly vertical, cracks of various directions also were reported. All of those cracks were secondarily filled with calcite, anhydrite, gypsum, or clay mass. There were no reports about the increased seismic activity before the event; and, moreover, there were no reports about any instability of the excavation and corridors near the fault zone. The active excavation works were carried out about 200–400 m from the fault zone.

We first investigate the rupture process on the base of local data, both using in-mine and surface recordings (see Fig. 1). Previous MTs using local data (Lizurek *et al.*, 2014), derived from first-motion polarities at in-mine stations and waveform

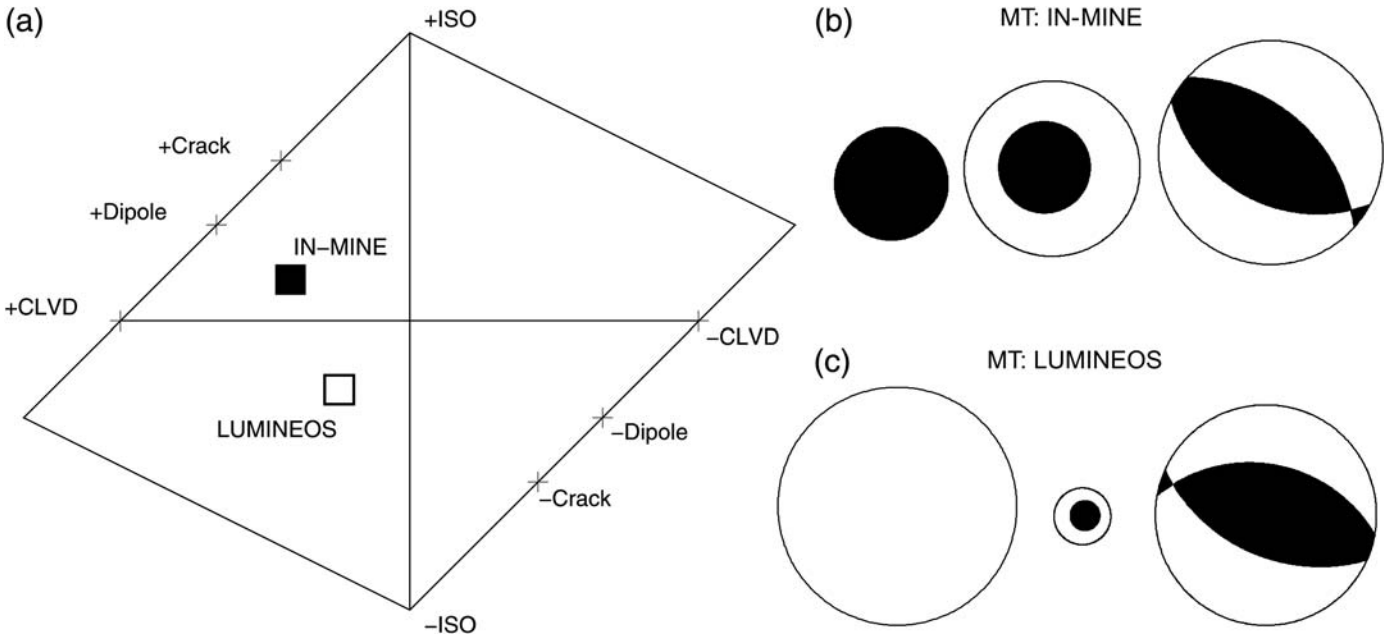

▲ **Figure 3.** (a) The Hudson source-type plot with two local solutions, moment tensor (MT) decompositions for isotropic (ISO), CLVD, and double-couple parts, (b) in-mine solution, and (c) LUMINEOS solution. The size of decomposed focal spheres scales to their contribution to the full MT (see also Ⓔ Table S2).

modeling at surface stations, were ambiguous (see Hudson source-type plot, Fig. 3a) and suggested a complex rupture: although both solutions present a northwest–southeast-oriented thrust-mechanism component, the MT derived from the in-mine network (Fig. 3b) suggested a dominant DC mechanism, accompanied by a positive compensated linear vector dipole (CLVD) and isotropic sources. The waveform modeling at surface stations instead indicated a stronger negative isotropic component (Fig. 3c). An implosive MT component could be controlled by the seismic signal associated with the rockburst, for which there was direct evidence in the mine. Apart from the disagreement among these solutions, the quality and robustness of both of them are questionable. On one side, the in-mine solution is only based on first-motion polarities, a method that has a poor resolution toward full MT inversion and that could be strongly affected by structural heterogeneities and cavities, which are unaccounted for in the 1D model approximation. On the other hand, the LUMINEOS solution is likely poorly constrained, because it was obtained on the basis of few recordings (only four sensors were available at the time of the earthquake) and with a large azimuthal gap. In these conditions, the additional constraints provided by the regional data are required to understand and model the complex rupture process.

THE 19 MARCH 2013 EVENT IN A REGIONAL VIEW

The regional MT inversion is performed using three-component recordings from Polish, German, and Czech permanent broadband seismic stations, all equipped with Streckeisen STS-2 high-gain very-broadband seismometers. Based on the azimuthal coverage, we chose the seven best-located stations around the source (Ⓔ Table S1 and Fig. 1a). Waveform data and station metadata were obtained from the Observatories and Research Facilities for European Seismology (ORFEUS) project (see Data and Resources). Data preprocessing included the deconvolution of the instrumental response to obtain true displacements and decimation to 5 Hz.

The MT inversion can be performed by comparing observed and synthetics seismograms either in the time domain or in the frequency domain (by fitting amplitude spectra). Approach based on amplitude spectra fitting is less sensitive to mismodeling of the velocity structure than time domain inversion (Cesca *et al.*, 2006; Domingues *et al.*, 2013). We chose to do this inversion in the frequency domain because it was previously tested for weak and shallow mining-induced events at local (Sen *et al.*, 2013) and regional (Cesca *et al.*, 2013) distances.

To compare synthetic and observed data, Green's functions and synthetic seismograms are built considering a 1D velocity model. The choice of the velocity model can partially affect the MT solution (see Domingues *et al.*, 2013), especially in combination with a poor azimuthal coverage. To ensure the quality of regional MT inversion results, we tested three different velocity models. One is based on the CRUST2.0 (Fig. 4a) database (Bassin *et al.*, 2000), and two are local velocity models of Poland: MM2012 (Fig. 4b) (Majdański, 2012) and GM2003 (Fig. 4c) (Grad *et al.*, 2003). All inversions were performed for a fixed source depth of 1 km, as constrained by the in-mine recordings and direct observations.

The regional data can be first used to assess the quality of the independent MT solutions obtained from the local network. If we compute synthetic displacement seismograms for the two

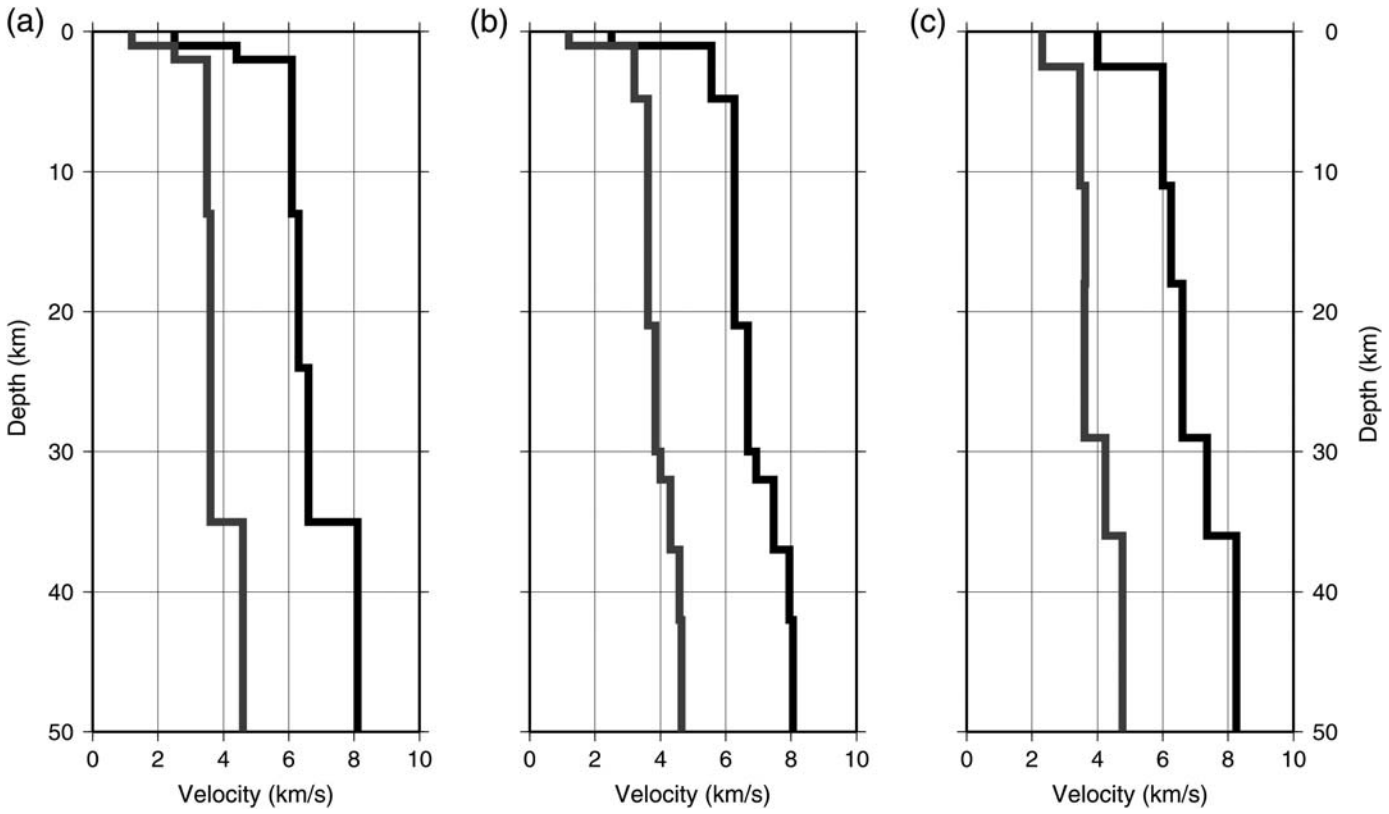

▲ **Figure 4.** Velocity models used during regional MT inversions based on: (a) regional model CRUST2.0 and two local models based on, (b) Majdański (2012) and (c) Grad *et al.* (2003).

locally derived source models from Figure 3b,c and Ⓔ Table S2, at seismic stations at regional distances, and compare them with observations, it turns out that the MT solution derived from the LUMINEOS network reproduce observations much better (Fig. 5a,b). The synthetic seismograms shown in Fig. 5a,b were obtained with the CRUST2.0 model; similar conclusions can be drawn when using the alternative models.

For the regional MT inversion, we use the Kiwi tools inversion platform (Heimann, 2011) and follow the inversion procedure described in Cesca *et al.* (2013), which is based on full waveform displacements and spectra in the frequency range, in our case filtered between 0.07 and 0.1 Hz. We further decompose the MT solution into DC, CLVD, and isotropic components. Such decomposition is the most commonly used in seismology (Jost and Hermann, 1989). Ⓔ Table S2 summarizes and compares MT results for both local and regional data. Regional solutions are all very similar and are characterized by a combination of a dominant negative isotropic term and a negative subvertical CLVD term. The similarity of MT results confirms the stability of the regional inversion, showing that, in our case, the MT solution is only marginally affected by the velocity model. The GM2003 model is the best one, with its MT best fitting the data.

The comparison of regional and local MT solutions (Ⓔ Table S2) shows some interesting features. The in-mine and regional solutions are extremely different and hardly explain a common process: the in-mine solution is controlled by a thrust DC component, which is negligible in the regional solution. Seismic moments also present differences, with the regional solutions characterized by higher magnitudes. The best-fitting regional solution has a magnitude of M_w 4.2, whereas local solutions have M_w 3.6.

The solution provided by the LUMINEOS network is treated separately, as a particular case, because its mechanism has features either compatible with the in-mine or the regional solution. The relatively high DC component, its thrust geometry, and its striking well match the in-mine MT result. Both local solutions are also similar in magnitude. On the other hand, the very high implosive isotropic term is in agreement with the regional solution. Here, we also test the consistency between synthetics calculated for the regional and LUMINEOS MT solutions with in-mine displacement traces observed on four nonsaturated stations. All signals were filtered in the 1–3 Hz passband, which corresponds to the flat response of the seismic sensor, below corner frequency. Figure 5c shows a comparison of first-arrival synthetic seismograms for the regional MT solution (bottom gray), LUMINEOS MT solutions (middle gray), and the original in-mine data (top black); we notice that, although synthetics for the regional MT are in disagreement with original data, the LUMINEOS MT solution predict relatively similar seismograms to those that were observed.

The apparent disagreement among these results could support the complex rupture model for the Rudna event. We propose a model to explain all discrepant results. In our model, the

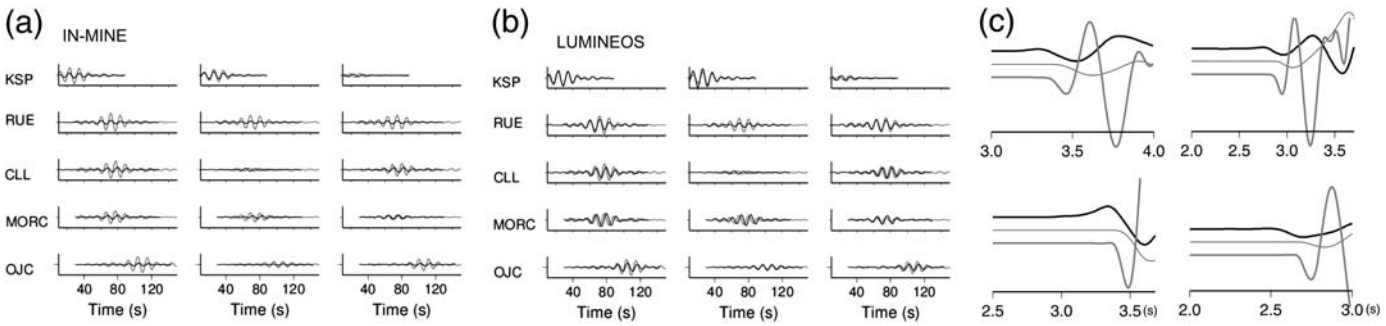

▲ **Figure 5.** Synthetics (black) and observed data (gray) at regional distances, when assuming two different solutions derived from local data, (a) fitting first-motion polarities at the in-mine network and (b) the full waveform of the LUMINEOS network. (c) Comparison of displacement traces between original in-mine data recorded on nonsaturated stations (top black) and synthetic traces estimated for regional MT solution on the considered in-mine stations (bottom gray). Synthetics for LUMINEOS MT are also included (middle gray).

rupture process was composed of different subevents, with different focal mechanisms and energy releases. In such a general scenario, when the rupture process takes place as two or more subevents, the polarity-based approach reveals only the geometry of the first nucleation process, whereas the low-frequency regional inversion procedure reveals the geometry and moment release of the strongest one. In our case, this would mean that the rupture nucleates as a mining-triggered thrust faulting and continues into a more energetic collapse.

SPECTRAL PARAMETER ANALYSIS

The hypothesis of a complex rupture scenario can also be independently investigated through the analysis of spectral parameters. A spectral analysis was performed to estimate source parameters such as seismic moment, seismic energy, radius, and slip. Seismic moment and energy were calculated using the Boore and Boatwright (1984) methodology, the source radius was obtained using the formalism of Brune (1970, 1971), and the circular fault model of Madariaga (1976) was used to calculate slip from seismic moment definition (Aki and Richards, 1980). Ⓔ Table S3 shows the derived spectral source parameters. In-mine network estimates are presented as average values obtained from the *P*-wave recordings on 20 stations and four recordings of unsaturated *S* waves (Lizurek *et al.*, 2014).

Local-station source parameters estimations, except the *S* and *P* spatial energy (E_S/E_P) ratio, are significantly smaller than the estimates derived from broadband stations based upon the same regional velocity model (Fig. 6). This is consistent with the significant difference among the scalar moment and magnitude derived from local and regional data. The E_S/E_P ratio observed at the LUMINEOS and in-mine stations is significantly higher than at regional broadband stations, which corresponds well with the obtained focal mechanisms. In fact, the presence of a strong DC component from local solutions predicts a larger E_S/E_P ratio, whereas this ratio decreases for the radially symmetric source radiation pattern inferred from the regional data.

The slip values estimated from stations located west of the epicenter are significantly higher than at those located eastward (Fig. 6). A comparable pattern is not visible for M_w and radius estimates. Instead, the observed corner frequency is significantly lower at western stations. These lateral asymmetries may be consequence of rupture directivity: higher frequencies, short apparent durations, larger apparent moment, and slip to the east, with respect to the west, could suggest an eastward propagation of the rupture process.

Regional broadband recordings are also dominated by low frequencies. This is a consequence of the high-frequency attenuation at regional distances but, according to our complex source model, also indicates a slower duration of the most energetic source process imaged at regional distances.

The general finding that local underground and surface stations show smaller M_w, slip, and radius values but higher E_S/E_P values is in agreement with the different focal mechanism solutions obtained from local and regional data and supports the complex rupture model.

COMPLEX RUPTURE MODELING FROM LOCAL AND REGIONAL DATA

The discrepancy among MT solutions and spectral source parameters derived by regional and local networks support a complex rupture model. We argued that the in-mine solution is providing evidence for the rupture geometry at the nucleation time, when the process is responsible for a low-energy signal, compatible with a DC source releasing a moment equivalent to M_w 3.6. Instead, the regional solution is characterized by strong implosive and vertical CLVD terms.

Such a high implosive component has been rarely observed and has a direct physical interpretation. Besides confirming the presence of a faulting structure in the hypocentral region, the direct inspection of the affected area in the mine after the occurrence of the seismic event gave obvious evidence for a collapse. The underground postseismic survey revealed that an important rockfall was accompanied by tunnel floor uplift (E. Koziarz, personal comm., 2013). In this condition, the collapse event should be best modeled as a tabular collapse (Aki and Richards, 1980; Talebi and Côté, 2005), a process that is sketched in Figure 7a, together with its theoretical *P*-wave radiation pattern (Fig. 7b).

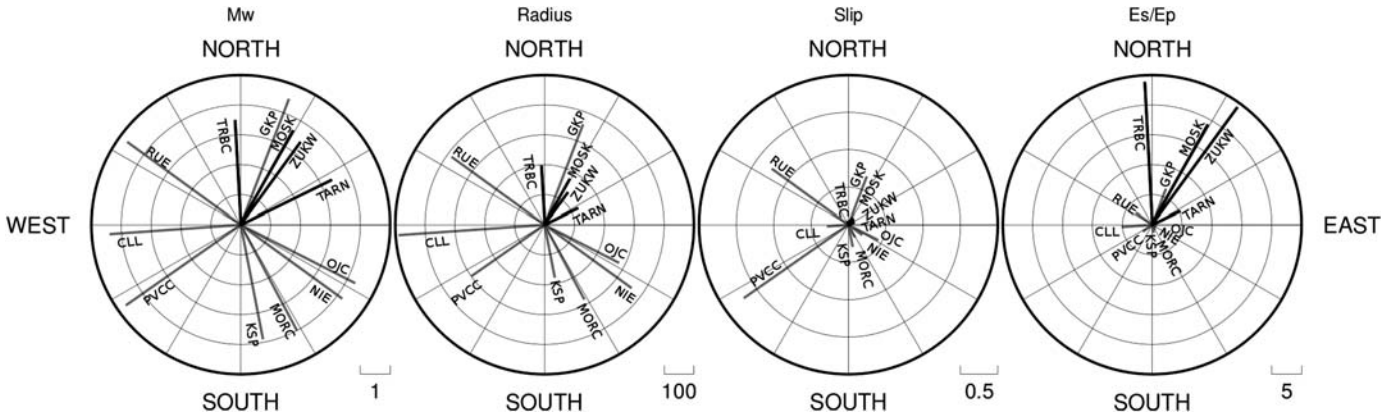

▲ **Figure 6.** Rose diagrams of M_w, radius, slip, and S and P spatial energy (E_S/E_P) ratio estimates versus azimuth of the station.

A tabular cavity with vertical displacement is analogous to a closing tensile crack model, in which the dipole magnitude ratio is $1 : 1 : (\lambda + 2\mu)/\lambda$ (λ and μ are Lamé constants). For a Poisson solid ($\lambda = \mu$) and assuming a vertical collapse, the nonzero elements of the resulting MT density are $m_{11} = m_{22} = -1$ and $m_{33} = -3$.

Figure 8 demonstrates how such a simple model alone can well reproduce observed displacements at regional distances. In this simulation, synthetic displacements were computed using a diagonal MT density with nonzero elements $m_{11} = m_{22} = -1$ and $m_{33} = -3$ and seismic moment $M_0 = 2 \times 10^{15}$ N·m, corresponding to moment magnitude M_w 4.1.

From the illustration of the radiation pattern of a tabular cavity (Fig. 7b), this model predicts dilatational first motion at all azimuths and incidence angles. This is in contradiction to local recordings within the mine, where both positive and negative onsets were depicted and where the overall polarities distribution was best modeled by a DC thrust mechanism. Our interpretation is that the regional inversion only reveals the tabular collapse signal, and thus the source model for the rockburst. Two possible factors might have contributed to the fact that the regional inversion is unable to detect the early thrust mechanism: the first one is that the collapse released much more energy than the triggering DC event, the second that its source was more effective in generating low-frequency signals at distances of 100–300 km, which could be possible if the collapse occurred at shallower depth or was characterized by a slower process. The first hypothesis is supported by the estimated scalar moments, with the in-mine data revealing an M_w 3.6 for the thrust event and the regional data suggesting M_w 4.2, which we can mostly attribute to the collapse. Whereas a significant depth difference among the thrust and collapse sources is ruled out by local postseismic observations, the additional influence of a slower rupture for the collapse process cannot be excluded. Our complex rupture model is supported by evidence from the visual inspection after the rockburst: the hypocentral location corresponds to a mapped fault with northwest–southeast geometry, also recognized by visual inspection, and it could be confirmed that the rockburst occurred as a tabular collapse accompanied by a floor uplift.

If a pure thrust explains the in-mine MT solution and a tabular collapse explains the regional MT solution, both mechanisms remain inconsistent with the MT result from the local surface LUMINEOS network, leaving open questions on its interpretation. The next section aims to answer these questions, providing an interpretation of the LUMINEOS MT results in the framework of the suggested complex rupture model.

MOMENT TENSOR DECOMPOSITION AND INTERPRETATION FOR COMPLEX EVENTS IN MINES

Until now, we had always decomposed all full MT inversion results into DC, CLVD, and isotropic terms using the most common decomposition. Among the several proposed MT decompositions (see Jost and Hermann, 1989, for a review), this decomposition is typically well accepted, because it uniquely separates the isotropic component and because it assumes the deviatoric component to be dominated by the DC term, with the CLVD being generally interpreted as an artifact of the inversion procedure for noisy data or poor monitoring conditions. The most relevant aspect of the DC− CLVD decomposition is that it forces the largest dipoles of the CLVD axis to have common orientation with the pressure or the tension axis of the DC fault, when the dipole is negative or positive respectively. For tectonic earthquakes, the focal mechanism orientation is controlled by the dominant DC term, and a remaining, spurious CLVD term will be oriented accordingly. The DC + CLVD decomposition may also work properly if the CLVD dominates the deviatoric component (e.g., for tensile crack sources) and the DC is marginal. In such case, the dominant CLVD term controls the source orientation of an eventual minor residual DC term.

However, as in this case study, this decomposition yields improper results whenever the source presents significant DC and CLVD terms that are each associated with different processes with no common geometry. In the present case, the DC term of the starting event is a thrust mechanism on a pre-existing fault and has a steep, subvertical T axis and a subhorizontal P axis. As it occurs, the subsequent collapse event has a vertical pressure

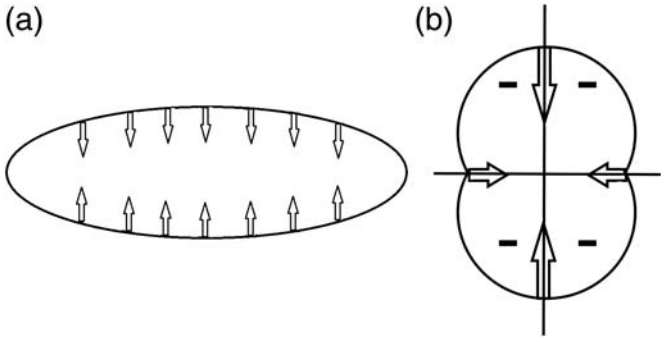

▲ **Figure 7.** (a) A sketch of the contraction of a tabular cavity (after Talebi and Côté, 2005) and (b) the corresponding. *P*-wave radiation pattern, in which minus signs correspond to dilatation (after Talebi and Côté, 2005).

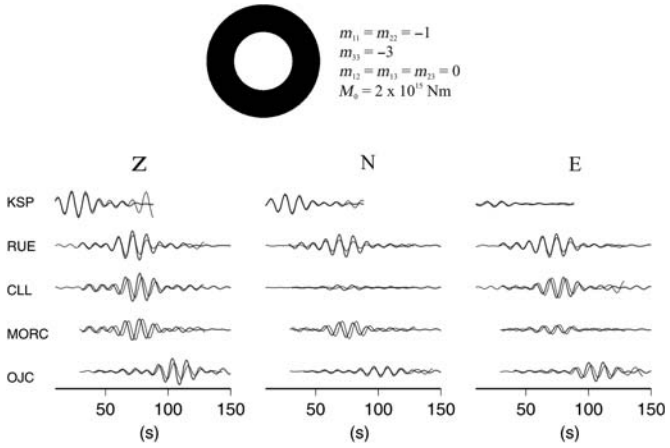

▲ **Figure 8.** Observed (gray line) and synthetic (black line) seismograms generated for the pure tabular cavity vertical displacement model on selected regional stations.

axis. If the LUMINEOS MT were able to reveal both these two basic processes, they could not be properly decomposed using the standard MT decomposition. This statement is easily demonstrated by building up a synthetic MT as the sum of a pure north–south thrust mechanism, with dip 45° and a pure vertical collapse, both with a common scalar moment. Decomposing such an MT with the standard decomposition, one obtains 41% negative isotropic term, 34% negative CLVD term, and 25% DC. The DC mechanism in this case has the proper orientation (i.e., it is consistent with the original thrust DC contribution), but the CLVD has an east–west orientation, constrained by the horizontal pressure axis of the DC term, and in no ways helps to infer that a collapse took place. Obviously this result can change, based upon the ratio of the scalar moments of the two original DC and collapse MTs.

We propose two alternative approaches to interpret collapse-related events, with potential applications at least in mining and volcanic environments: an MT decomposition and an MT fitting procedure. Both approaches assume that a vertical collapse occurs and can be modeled as for a tabular collapse, with the MT density configuration as described in the previous section.

In the first case, we perform an MT decomposition following a similar approach as Ford *et al.* (2008), in which the original full MT is represented as the sum of a vertical collapse (here with dipoles ratio 1:1:3), which is the sum of a negative isotropic and a CLVD with a negative vertical major dipole, and a deviatoric term, which can be further decomposed into a DC and a second CLVD term:

$$M = M^{\text{Collapse}} + M^{\text{Deviatoric}} = (M^{\text{ISO}} + M^{\text{CLVD}}) + (M^{\text{DC}} + M^{\text{CLVD}}), \quad (1)$$

in which M^{Collapse} is a diagonal terms with elements $\{-0.2\,\text{Tr}(M), -0.2\,\text{Tr}(M), -0.6\,\text{Tr}(M)\}$, defined upon the trace of the original MT. The determination of a collapse term, with negative value entry of diagonal elements, is only possible if the original MT has a negative isotropic component. However, the decomposition can be generalized to arbitrary signs of the isotropic component, as the sum of a horizontal tensile crack (a closing horizontal tensile crack corresponds to the collapse of a tabular cavity) and a deviatoric term.

As an alternative to this decomposition of the full MT, we propose to search for the optimal combination of a vertical-collapse MT and a DC MT with arbitrary orientation, so that the sum of their MTs is able to reproduce the original MT, by minimizing the difference to the original MT entries. The suggested inversion procedure is simple: (1) iteratively scan the range of possible DC orientations; (2) assuming it is possible to represent the target full MT M as

$$M_{ij} = M_0^{\text{DC}} m_{ij}^{\text{DC}} + M_0^{\text{Collapse}} m_{ij}^{\text{Collapse}} + \varepsilon, \quad (2)$$

perform a matrix inversion (generalized inverse) to solve for the best scalar moments (M_0^{DC} and M_0^{Collapse}) of the DC and collapse MTs; and (3) estimate the residuals ε. The orientation of the DC is found where the residuals ε are minimized.

Both approaches present different advantages. The decomposition method might be preferred when the isotropic component is safely derived. In the presence of relevant uncertainties on the overall isotropic components, for example, if important trade-offs between different MT components and/or the CLVD–isotropic terms cannot be resolved, the second procedure may be more stable.

We tested both methods to interpret the MT configuration retrieved by the LUMINEOS network at local distances (Ⓔ Table S2). The scalar moments of the collapse component resolved in both cases is equivalent to a moment magnitude M_w 3.8 and thus slightly underestimates the independent regional MT inversion. The minor discrepancy may arise by the slow emission of energy during the rockburst process. In such conditions, the low-frequency regional amplitude spectra MT inversion estimate should be more efficient in capturing the energy released by a slow process, and the resulting slightly higher scalar moment can be considered a better estimate.

The resolved DC component has an orientation of strike 295°, dip 42°, and rake 86° for the MT decomposition and strike 284°, dip 42°, and rake 84° for the MT fitting procedure. Both results are in good agreement with those derived at local distances, and are extremely consistent with the MT that was independently resolved by the LUMINEOS network (strike 285°, dip 42°, rake 83°). In the decomposition approach, the DC term (41% of the deviatoric MT) is accompanied by a CLVD with vertical positive maximal dipole, which also is consistent with the deviatoric MT result from in-mine data. The magnitude of the resolved-thrust DC term varies between M_w 3.6 (MT decomposition) and 3.8 (MT fitting procedure). The lower bound seems more realistic, because it well matches the estimations from in-mine data and explains why this component is not resolved by the regional data inversion, which is controlled by the more energetic collapse process (with a scalar moment about 10 times larger).

Both approaches indicate that the LUMINEOS MT could result from the superposition of two main terms, a thrust DC and a pure collapse model. These two terms are compatible with the source models independently derived by the local in-mine and the broadband regional stations, respectively. Although we can prove that the LUMINEOS network has the potential to resolve the whole complex rupture process, a standard MT decomposition would still fail to reveal that the rupture process was actually composed of two subevents. A proper MT interpretation can be carried out using one of the proposed decomposition approaches.

CONCLUSIONS

The 19 March 2013 seismic event at the Rudna copper mine has been characterized by a complex rupture history, starting with a weaker M_w 3.6 thrust mechanism and continued with a more energetic M_w 4.2 collapse. The nucleation process took place along a known fault structure, as directly verified in the mine during an inspection. The occurrence of a thrust failure along a fault classified as normal suggests a significant rotation of the local stress field before the event, as a result of the mining exploitation. The following collapse and rockfall, also verified by visual inspection of the accident site, were responsible for important damage and trapped miners. Despite the apparent ambiguity among local and regional MT inversion solutions, the complex rupture can be well tracked, considering that first-motion polarities at local distances only provide information on the nucleation phase and thus only reveal the thrust mechanism geometry. Regional stations, in contrast, can only image the most energetic source term, here the following collapse process. The obtained mechanism solutions discrepancy was thus not due to an instability of moment inversion routines, but originated by the complex rupture. The spectral analysis further supported the interpretation of a complex event: the spectral estimates of M_0 and M_w, slip and radius of the event are significantly higher in the case of regional stations, where they are controlled by the more energetic low-frequency waves associated with the collapse. Moreover, the implosive character of the main part of the event is confirmed by E_S/E_P ratio estimations, which are significantly lower for regional stations.

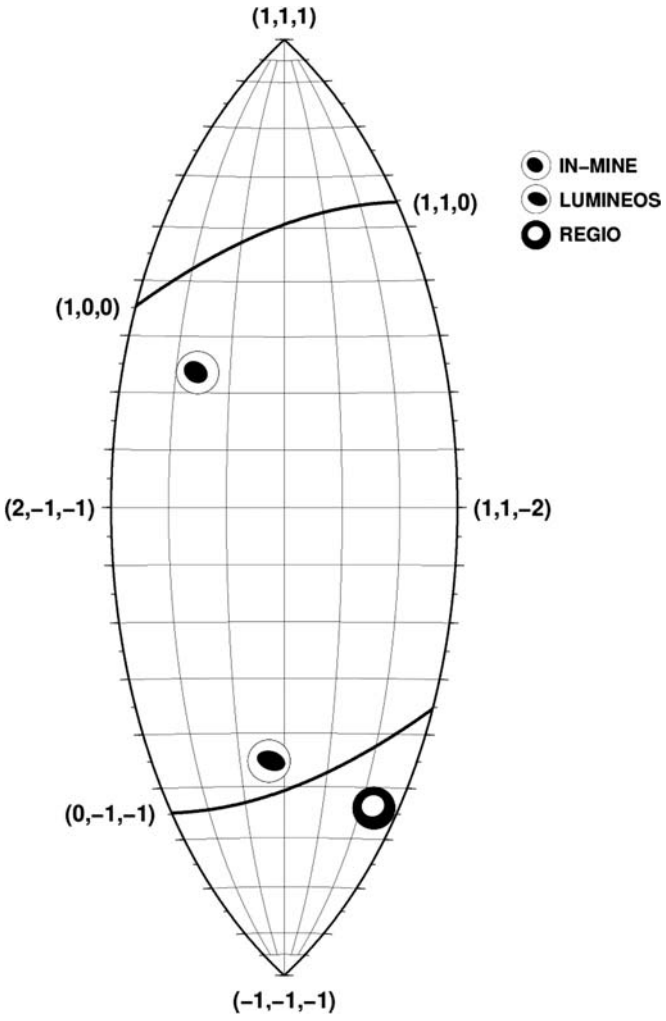

▲ **Figure 9.** Source-type plot (Tape and Tape, 2012) with two subevents clearly visible: the first is recorded in the first *P*-wave arrivals (recorded by the in-mine network), and the second was responsible for the rockburst (recorded by LUMINEOS and regional networks).

The surface installation at local distances offers a chance to detect the whole process and both subevents. Given their close location to the seismic source, they can detect high frequency and weaker amplitudes associated with the first event, which are attenuated at larger distances and/or hidden in the higher amplitude rockfall signal. At the same time, data were not clipped and also include the signal of the rockfall. However, we showed that the usage of a standard MT decomposition hides the dual nature of this rupture process, because of the intrinsic constraints on the geometry of DC and CLVD terms.

Figure 9 shows a source-type diagram (Tape and Tape, 2012) displaying the mechanisms of the two subevents, the first one revealed by the in-mine inversion and the second one fully explained by the regional solution. The plot illustrates how the

LUMINEOS solution can be seen as a combination of these two solutions.

To overcome the difficult interpretation of standard decomposition, we used an alternative decomposition and proposed a new fitting procedure. Both can help to resolve complex rupture processes, including collapse sources. The application of these methods to the LUMINEOS full MT solution illustrates that this was, in fact, consistent with the composition of the two MT solutions obtained from local in-mine and regional installations. It should be noted that these approaches also have a significant impact on the seismic moment estimates, because the sum of the moment associated with the collapse and deviatoric terms differs from the scalar moment obtained by a standard decomposition. Here we should emphasis some practical issues that follow this study. The first consideration concerns the limitations of the typical low-dynamic range of seismic networks in mining environments. Our analysis shows that the dynamic range plays a primary role in case any more sophisticated full waveform seismological analysis is desired; in standard conditions, the recording of in-mine data alone, may not provide sufficient information for this type of studies. A second consideration is that a strong and hazardous event could happen without any predicting seismological signal, even if the earthquake is directly connected with a well-known fault zone. Even though seismological methodology to predict such hazardous events is not available, knowledge about its mechanism (even *post factum*) brings crucial knowledge for the engineers about how to avoid dangerous circumstances in planning future works in the vicinity of similar fault zones. Our general conclusion is that fault zones far from the mining front that are considered as stable should be carefully monitored (e.g., by geodetic survey), because stress accumulation still plays a big role on such tectonic discontinuities. Beside obvious applications to mining environments, these approaches may have important applications also in volcanic areas where, as with mining seismology, non-DC sources are commonly observed.

DATA AND RESOURCES

In-mine seismic data and technical information on the Rudna mine were obtained for this study with kind permission of KGHM, Polska Miedź S.A. The LUMINEOS data set belongs to the Institute of Geophysics Polish Academy of Sciences, and regional seismic data were accessed through the repository of the Observatories and Research Facilities for European Seismology (ORFEUS) project at http://www.orfeus-eu.org/data.html (last accessed January 2016). Regional moment tensor inversions were obtained with the Kiwi tools inversion platform (http://kinherd.org, last accessed January 2016). Figures were prepared using the Generic Mapping Tools package (Wessel and Smith, 1998).

ACKNOWLEDGMENTS

Łukasz Rudziński and Grzegorz Lizurek have been partially supported by project IS-EPOS Digital Research Space of Induced Seismicity for EPOS Purposes (POIG.02.03.00-14-090/13-00), funded by the Polish National Center for Research and Development, as well as within statutory activities Number 3841/E-41/S/2015 of the Ministry of Science and Higher Education of Poland. Simone Cesca has been partially funded by the MINE project (German BMBF Geotechnologien programme, Grant of Project BMBF03G0737A). We wish to express our gratitude to Editor Zhigang Peng. The authors are also indebted to Sean Ford and an anonymous reviewer for their valuable comments, which considerably improved this paper.

REFERENCES

Aki, K., and P. G. Richards (1980). *Quantitative Seismology*, W.H. Freeman, San Francisco, California.

Baker, C., and R. P. Young (1997). Evidence for extensile crack initiation in point source time-dependent moment tensor solutions, *Bull. Seismol. Soc. Am.* **87,** no. 6, 1442–1453.

Bassin, C., G. Laske, and G. Masters (2000). The current limits of resolution for surface wave tomography in North America, *Eos Trans. AGU* **81,** no. 48 (Fall Meet. Suppl.), Abstract S12A–03.

Boore, D. M., and J. Boatwright (1984). Average body-wave radiation coefficients, *Bull. Seismol. Soc. Am.* **74,** 1615–1621

Brune, J. N. (1970). Tectonic stress and the spectra seismic shear waves from earthquakes, *J. Geophys. Res.* **75,** 4997–5009.

Brune, J. N. (1971). Correction, *J. Geophys. Res.* **76,** 5002.

Cesca, S., E. Buforn, and T. Dahm (2006). Moment tensor inversion of shallow earthquakes in Spain, *Geophys. J. Int.* **166,** no. 2, doi: 10.1111/j.1365-246X.2006.03073.x.

Cesca, S., A. Rohr, and T. Dahm (2013). Discrimination of induced seismicity by full moment tensor inversion and decomposition, *J. Seismol.* **17,** no. 1, 147–163, doi: 10.1007/s10950-012-9305-8.

Cichowicz, A. (2000). Quantification of complex seismic sources, in *Rockburst and Seismicity in Mines*, G. van Aswegen, R. J. Durrheim, and W. D. Ortlepp (Editors), The South African Institute of Mining and Metallurgy, Johannesburg, South Africa, 91–97.

Dahm, T., G. Manthei, and J. Eisenblätter (1999). Automated moment tensor inversion to estimate source mechanisms of hydraulically induced microseismicity in salt rock, *Tectonophysics* **306,** no. 1, 1–17, doi: 10.1016/S0040-1951(99)00041-4.

Dębski, W., B. Guterch, H. Lewandowska-Marciniak, and P. Labák (1997). Earthquake sequences in the Krynica region, western Carpathians, 1992–1993, *Acta Geophysica Polonica* **45,** 255–290.

Domanski, B. M. (2007). Source parameters of the 2004 Kaliningrad earthquakes, *Acta Geophysica* **55,** no. 3, 267–287, doi: 10.2478/s11600-007-0021-7.

Domingues, A., S. Custodio, and S. Cesca (2013). Waveform inversion of small to moderate earthquakes located offshore southwest Iberia, *Geophys. J. Int.*, doi: 10.1093/gji/ggs010.

Dreger, D. S., S. R. Ford, and W. R. Walter (2008). Source analysis of the Crandall Canyon, Utah, mine collapse, *Science* **321,** 217, doi: 10.1126/science.1157392.

Fletcher, J. B., and A. McGarr (2005). Moment tensor inversion of ground motion from mining-induced earthquakes, *Bull. Seismol. Soc. Am.* **95,** 48–57, doi: 10.1785/0120040047.

Ford, S. R., D. S. Dreger, and W. R. Walter (2008). Source characterization of the August 6, 2007 Crandall Canyon mine seismic event in central Utah, *Seismol. Res. Lett.* **79,** no. 5, 637–644, doi: 10.1785/gssrl.79.5.637.

Ford, S. R., D. S. Dreger, and W. R. Walter (2009). Identifying isotropic events using a regional moment tensor inversion, *J. Geophys. Res.* **114,** no. B01306, doi: 10.1029/2008JB005743.

Gibowicz, S. J. (1990). Seismicity induced by mining, *Adv. Geophys.* **32,** 1–74, doi: 10.1016/S0065-2687(08)60426-4.

Gibowicz, S. J. (2009). Seismicity induced by mining: Recent research, *Adv. Geophys.* **51,** 1–53, doi: 10.1016/S0065-2687(00)80007-2.

Grad, M., S. L. Jensen, G. R. Keller, A. Guterch, H. Thybo, T. Janik, T. Tiira, J. Yliniemi, U. Luosto, G. Motuza, *et al.* (2003). Crustal structure of the trans-European suture zone region along POLONAISE'97 seismic profile P4, *J. Geophys. Res.* **108,** doi: 10.1029/2003JB002426.

Hasegawa, H. S., R. J. Wetmiller, and D. J. Gendzwill (1989). Induced seismicity in mines in Canada–An overview, *Pure Appl. Geophys.* **129,** 423–453.

Heimann, S. (2011). A robust method to estimate kinematic earthquake source parameters, *Ph.D. Thesis*, University of Hamburg, Germany.

Jost, M. L., and R. B. Hermann (1989). A student's guide to and review of moment tensors, *Seismol. Res. Lett.* **60,** 37–57, doi: 10.1785/gssrl.60.2.37.

Lizurek, G., and P. Wiejacz (2011). Moment tensor solution and physical parameters of selected recent seismic events at Rudna Copper Mine, in *Geophysics in Mining and Environmental Protection*, A. F. Idziak and R. Dubiel (Editors), Geoplanet: Earth and Planetary Sciences 2, Springer, Heidelberg, Germany, doi: 10.1007/978-3-642-19098_12.

Lizurek, G., B. Plesiewicz, P. Wiejacz, J. Wiszniowski, and J. Trojanowski (2013). Seismic event near Jarocin, Poland, *Acta Geophys.* **61,** no. 1, 26–36, doi: 10.2478/s11600-012-0052-6.

Lizurek, G., Ł. Rudziński, and B. Plesiewicz (2014). Mining induced seismic event on inactive fault, *Acta Geophys.* doi: 10.2478/s11600-014-0249-y.

Madariaga, R. (1976). Dynamics of expanding circular fault, *Bull. Seismol. Soc. Am.* **66,** 639–666.

Majdański, M. (2012). The structure of the crust in TESZ area by Kriging interpolation, *Acta Geophys.* **60,** no. 1, 59–75, doi: 10.2478/s11600-011-0058-5.

Malovichko, A. A. (2005). Study of "low-frequency" seismic events sources in the mines of the Verkhnekamskoye potash deposit, in *Controlling Seismic Risk. Rockburst and Seismicity in Mines*, Y. Potvin and M. Hudyma (Editors), Australian Centre for Geomechanics, Nedlands, Australia, 373–377.

McGarr, A. (1992a). An implosive component in the seismic moment tensor of a mining-induced tremor, *Geophys. Res. Lett.* **19,** no. 15, 1579–1582, doi: 10.1029/92GL01581.

McGarr, A. (1992b). Moment tensors of ten Witwatersrand mine tremors, *Pure Appl. Geophys.* **139,** 781–800, doi: 10.1007/BF00879963.

Richardson, E., A. A. Nyblade, W. R. Walter, and A. J. Rodgers (2005). Source characteristics of mining-induced seismicity from moment tensor analysis and spatio-temporal relationship, in *Controlling Seismic Risk. Rockburst and Seismicity in Mines*, Y. Potvin and M. Hudyma (Editors), Australian Centre for Geomechanics, Nedlands, Australia, 123–127.

Riemer, K. L. (2005). Interpreting complex waveforms from some mining related seismic events, in *Controlling Seismic Risk. Rockburst and Seismicity in Mines*, Y. Potvin and M. Hudyma (Editors), Australian Centre for Geomechanics, Nedlands, Australia, 247–257.

Sen, A. T., S. Cesca, M. Bischoff, T. Meier, and T. Dahm (2013). Automated full moment tensor inversion of coal mining-induced seismicity, *Geophys. J. Int.* **195,** 1267–1281, doi: 10.1093/gji/ggt300.

Sprenke, K. F., B. G. White, A. C. Rohay, J. K. Whyatt, and M. C. Stickney (2002). Comparison of body-wave displacement with damage observations of rockburs, Coeur d`Alene Mining District, Idaho, *Bull. Seismol. Soc. Am.* **92,** 3321–3328, doi: 10.1785/0120010105.

Stec, K. (2007). Characteristics of seismic activity of the Upper Silesian Coal Basin in Poland, *Geophys. J. Int.* **168,** no. 2, 757–768, doi: 10.1111/j.1365-246X.2006.03227.x.

Talebi, S., and M. Côté (2005). Implosional focal mechanisms in a hard-rock mine, in *Controlling Seismic Risk. Rockburst and Seismicity in Mines*, Y. Potvin and M. Hudyma (Editors), Australian Centre for Geomechanics, Nedlands, Australia, 113–121.

Tape, W., and C. Tape (2012). A geometric comparison of source-type plots for moment tensors, *Geophys. J. Int.* **190,** 499–510, doi: 10.1111/j.1365-246X.2012.05490.x.

Teyssoneyre, V., B. Feignier, J. Šileny, and O. Coutant (2002). Moment tensor inversion of regional phases: Application to a mine collapse, *Pure Appl. Geophys.* **159,** 111–130, doi: 10.1007/978-3-0348-8179-1_5.

Vavryčuk, V., and D. Kühn (2012). Moment tensor inversion of waveforms: A two-step time-frequency approach, *Geophys. J. Int.* **190,** 1761–1776, doi: 10.1111/j.1365-246X.2012.05592.x.

Wessel, P., and W. H. F. Smith (1998). New, improved version of Generic Mapping Tools released, *Eos Trans. AGU* **79,** 579.

Whidden, K., Ł. Rudziński, G. Lizurek, and K. L. Pankow (2013). Regional, local, and in-mine moment tensor for the 2013 Rudna Mine collapse, Poland, *Eos Trans. AGU* (Fall Meet. 2013), Abstract S21-2396.

Wiejacz, P., and W. Dębski (2009). Podhale, Poland, earthquake of November 30, 2004, *Acta Geophys.* 57**,** no. 2, 346–366, doi: 10.2478/s11600-009-0007-8.

Wiejacz, P., and Ł. Rudziński (2010). Seismic event of January 22, 2010 near Bełchatów, Poland, *Acta Geophys.* **58,** no. 6, 988–994, doi: 10.2478/s11600-010-0030-9.

Łukasz Rudziński
Grzegorz Lizurek
Institute of Geophysics
Polish Academy of Sciences
ul. Ks. Janusza 64
01-452 Warszawa
Poland
rudzin@igf.edu.pl

Simone Cesca
GFZ German Research Centre for Geosciences
Telegrafenberg
D-14473 Potsdam, Germany
cesca@gfz-potsdam.de

Published Online 3 February 2016